Unravelling the Microscopic Origin of Triplet Lasing from Organic Solids

Lopa Paul,[1]Ambar Banerjee,[2]Ankan Paul,[2] Kenneth Ruud[3] and Swapan Chakrabarti[1,]*

[1]Department of Chemistry, University of Calcutta

92, A.P.C. Road, Kolkata 700 009

India

[2]Raman Centre for Atomic Molecular and Optical Sciences, Indian Association for the Cultivation of Science,

2A & 2B Raja S C Mullick Road, Kolkata 700032

India

[3]Hylleraas Centre for Quantum Molecular Sciences, Department of Chemistry, University of Tromsø – The Arctic University of Norway

Tromsø N-9037, Norway

AUTHOR INFORMATION

Corresponding Author

*E-mail: swcchem@caluniv.ac.in Fax: 91-33-23519755

ABSTRACT: We present a heuristic mechanism for the origin of the unusual triplet lasing from (E)-3-(((4-nitrophenyl)imino)methyl)-2H-thiochroman-4-olate.BF_2.We demonstrate that whereas the moderate lifetime (1.03μs) of the first triplet state(T_1) prohibits triplet-triplet annihilation, the relatively faster $S_1 \rightarrow T_1$intersystem crossing and the 10^4 times smaller reverse intersystem crossing effectively help achieve population inversion in theT_1 state. Furthermore, the triplet lasing wavelength (675 nm) for the tetramer does not overlap with the triplet-triplet absorptions wavelength, indicating that the spin-forbidden emission cross section is very large. Additionally, the almost complete absence of a vibrational progression in the vibronic phosphorescence spectrum of the monomer plays an important role in ensuring efficient triplet-state lasing from this organic material. Our results show that controlling the triplet-state lifetimes combined with lowering of the triplet-triplet absorption in the emission region and small vibronic coupling will be the key steps when designing novel organic triplet-lasing materials.

TOC GRAPHICS

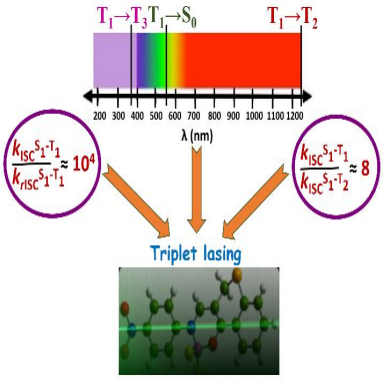

The three- to four-fold enhancement of the internal electroluminescence quantum efficiency of organic phosphorescent molecules[1-3] compared to their fluorescent analogues has made triplet lasing from organic solid-state lasers (OSSLs)[4,5] an active research field. However, achieving triplet lasing is difficult since it is very hard to achieve a population inversion of the $T_1$and S_0 states. This is mainly attributed to the pump-rate-induced singlet-singlet and singlet-triplet annihilations.[6,7] In addition, the weak spin-orbit coupling[8,9] in organic materials prohibits both efficient $S_1 \rightarrow T_1$ intersystem crossing (ISC) and $T_1 \rightarrow S_0$ phosphorescence, preventing appreciable optical gain to be achieved. Triplet lasing may furthermore be hindered by the ultralong phosphorescence lifetime-driven triplet-triplet annihilation (TTA)[10,11] and the overlap of the spin-allowed $T_1 \rightarrow T_n$ absorption with the phosphorescence spectrum.

Despite all these obstacles, Yu et al.[6] recently reported the first observation of triplet lasing from a nanowire microcavity of a metal-free organic compound. The phosphor is a sulfide-substituted difluoroboron compound,(E)-3-(((4-nitrophenyl)imino)methyl)-2H-thiochroman-4-olate.BF_2 (S-BF_2) which is derived from its parent compound (E)-2-(((4-nitrophenyl)imino)methyl)-naphthalene-1-olate.BF_2 (C-BF_2). The structures of S-BF_2 and C-BF_2 are shown in Figure 1. According to Yu et al.,[6] the motivation for the sulfur substitution in S-BF_2 was to increase the spin-orbit interactions between theS_1 andT_1 states vis-à-vis the ISC rate, a fundamental step towards triplet emission and finally triplet lasing from the S-BF_2 nanowire Fabry-Perot microcavity[12] under pulsed excitation. This unique experimental observation certainly raises questions of whether triplet lasing from this material is fortuitous or whether there are deeper microscopic origins for this unprecedented phenomenon. Unfortunately, the work of Yu et al.[6] does not shed light on these questions.

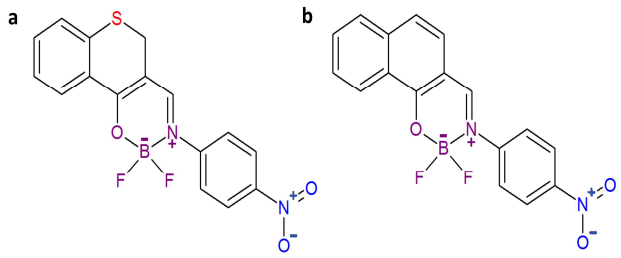

Figure 1. Structure of (a) S-BF2 and (b) C-BF2.

In this letter, we present a detailed theoretical analysis that explains the molecular origin of both phosphorescence and triplet lasing from S-BF_2. Since time-dependent density functional theory (TDDFT)[13]fails to determine the phosphorescence wavelength of the S-BF_2 molecule, we rely on the more accurate CASSCF/NEVPT2[14] method in combination with Dunning's cc-pVDZ basis set.[15] In addition, CASSCF/NEVPT2 provides a robust framework to compute spin-orbit interactions, and we here use the full Breit-Pauli relativistic Hamiltonian.[16] A four electron in four orbitals (4,4) active space has been adopted for all the computations (see Figure 2). With the (4,4) active space, state-averaged (SA)-CASSCF calculations are carried out for three singlet and two triplet-excited states. To investigate the triplet-triplet excitations explicitly, we have performed additional calculations considering the first three triplet states. It is to be noted that all the computations are performed using CH_2Cl_2 as a solvent in the framework of the CPCM model.[17] The computational details are provided in the Supporting Information.

From an inspection of the configuration-state functions (CSFs) and the corresponding coefficients of the wave functions for various states obtained from the SA-CASSCF computation, the $S_0 \rightarrow S_1$ or $S_1 \rightarrow S_0$ transition is found essentially to be a HOMO to LUMO transition (see Figure 2a) where the HOMO and LUMO orbitals are π- and π*-like orbitals, respectively. However, in the T_1 optimized geometry, HOMO-1 and HOMO showed an increase

in the contribution from the p orbitals of the S atom, thus extending these orbitals beyond the pure π-orbital framework. Whereas the S_0 state has primarily single-reference character, both the S_1 and T_1 states have some multi-reference character, explaining the breakdown of TDDFT in predicting the phosphorescence wavelength and transition moment of S-BF_2. It is also worth noting that the involvement of the p orbitals of the sulfur atom in the HOMO-1 and HOMO orbitals of the T_1 state could be the origin of the relatively larger spin-orbit coupling (SOC) between the S_1 and T_1 states of S-BF_2. In particular, it has been found that whereas the p_x orbital(10.1%) of the S atom has the largest contribution to the HOMO, it is the p_y orbital(8.9%) that actually makes the larger contribution in the HOMO-1. However, we did not find any S_1 (n↑,π*↓)-T_1(π,π*) character that could lead to an El-Sayed's rule-guided 100% efficient ISC, as claimed by Yu *et al.*[6] Moreover, the separation of the spin channels for the S_1 state (n↑,π*↓) in a spin restricted DFT/TDDFT calculation can not be realized.

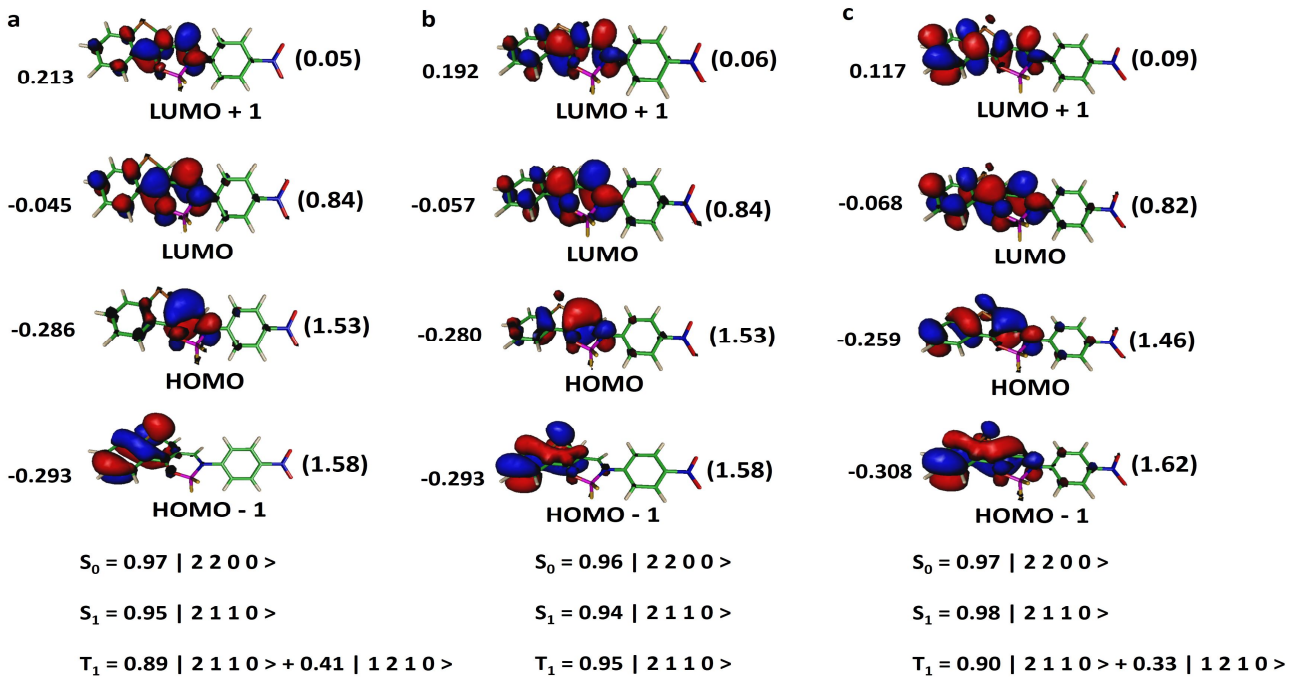

S_0 = 0.97 | 2 2 0 0 >

S_1 = 0.95 | 2 1 1 0 >

T_1 = 0.89 | 2 1 1 0 > + 0.41 | 1 2 1 0 >

S_0 = 0.96 | 2 2 0 0 >

S_1 = 0.94 | 2 1 1 0 >

T_1 = 0.95 | 2 1 1 0 >

S_0 = 0.97 | 2 2 0 0 >

S_1 = 0.98 | 2 1 1 0 >

T_1 = 0.90 | 2 1 1 0 > + 0.33 | 1 2 1 0 >

Figure 2. State averaged CASSCF optimized Molecular Orbitals (MO) for (a) S_0, (b) S_1 and (c) T_1-optimized geometries of S-BF_2. The corresponding orbital energies (Hartree) are provided on the left side of each MO and the occupation numbers are given in parenthesis. The CASSCF wave functions for the S_0, S_1 and T_1 states with the most dominant CSF and along with their corresponding weights are given below.

To inspect the possible phosphorescence process in C-BF_2, we have first calculated the SOC matrix elementbetween the S_1 and T_1 states using the same level of theory as for S-BF_2. A significantly lower value of 0.7 $cm^{-1}$is obtained, the square of which is almost 85 times smaller than that of S-BF_2 (6.4 cm^{-1}). This is consistent with the reported singlet oxygen generation efficiencies of S-BF_2 and C-BF_2which were found to be 98 % and 4%, respectively.[6]Since the probability of ISC-driven population gain of the T_1 state of C-$BF_2$is extremely low as compared to S-BF_2, we focus in the following on the S-BF_2system.

The calculated $S_0 \rightarrow S_1$ absorption, the $S_1 \rightarrow S_0$ fluorescence and the$T_1 \rightarrow S_0$ phosphorescence wavelengths of S-BF_2 are 410 nm, 509 nm and 564 nm, respectively, while the experimental wavelengths for absorption and phosphorescence in 1×10^{-5} M CH_2Cl_2 solution are 440 nm and 575 nm, respectively. It is also to be noted that $S_0 \rightarrow S_2$ absorption is the most intense one and it appears at a wavelength of 340 nm, which can be compared to the corresponding experimental value of 380 nm.The photoluminescence spectrum of S-BF_2in the solid state finds fluorescence and phosphorescence peaks at 510 nm and 610 nm, respectively, and we later return to this issue. The computed phosphorescence spectra agree well with the experimentally observed solution-phase spectra (Figure 3). The calculated $S_0 \rightarrow S_1$ absorption wavelength is underestimated by 30

nm. The exact wavelength depends on the choice of active space, but for consistency, we here only consider the results obtained with the (4,4) CAS wave functions.

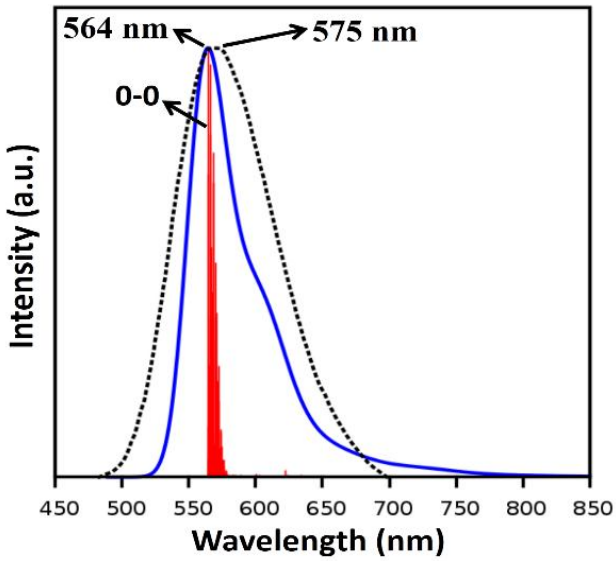

Figure 3. Experimental phosphorescence spectrum (black), vibrationally resolved simulated phosphorescence spectrum with fwhm=1000 cm^{-1}(blue), and stick spectrum assigning the 0-0 transition (red) of S-BF_2.

In order to understand the photo-physical dynamics associated with the phosphorescence and triplet lasing properties of S-BF_2, the calculation of rate constants of radiative and various non-radiative processes are important, and it is well known that molecular vibrations often play a significant role in determining the value of these rate constants. To validate the influence of vibronic coupling,[18,19] we calculated the Franck-Condon (FC) overlap integral involving all the normal modes of the molecule (details given in the Supporting Information). The FC vibronic spectrum simulated with full width at half-maximum (fwhm) = 1000 cm^{-1} is presented in Figure 3. Figure 3 shows that except for the 0-0 band, all other vibrational modes have negligible

intensity. It has previously been found[20] that when going from the monomer to the dimer, vibronic progressions in organic phosphorescent molecules decrease considerably due to poor spatial overlap of the vibrational wave functions representing different normal modes, suggesting that vibronic coupling-induced spectral broadening will be quenchedin crystallineS-BF_2. This important *in silico* observation suggests that lasing action from the T_1 state of S-BF_2 originates from the 0-0 transition without having any 0-1 component, and the four levels involved in the lasing process are thus S_0-S_2-S_1-T_1.

To get further insight into the lasing mechanism, we now examine the most important step in this process, namely the $S_1 \rightarrow T_1$ ISC process. The energy gap and the spin−orbit interaction between these states are the two major factors facilitating ISC.[21,22]The calculated $\Delta E_{S_1\text{-}T_1}$is 0.24 eV, and the SOC constant is 6.4 cm^{-1}. k_{ISC} is determined using Marcus−Levich−Jortner theory[23] derived in the framework of Fermi's golden rule[24] and is given by

$$k_{ISC} = \frac{2\pi}{\hbar}\left\langle T_1 \middle| H_{SOC} \middle| S_1 \right\rangle^2 \times \text{FCWD} \qquad (1)$$

where the first term represents the square of the SOC matrix element and the second term gives the Franck−Condon-weighted density of states (FCWD). The FCWD depends on the dimensionless electron−phonon coupling strength (the Huang−Rhys factor (S)[25]) overall the normal modes, reorganization energy, mode frequencies, and the energy difference between the states involved (see the Supporting Information). The calculated k_{ISC}achieved for S_1−T_1 using equation 1 is $2.26 \times 10^9 s^{-1}$ (Table 1).

The considerable ISC between the S_1 and T_1 states indicates a population growth of the latter state, but a competitive rISC between the states could cause population decay, leading to thermally activated delayed fluorescence (TADF).[26] The expression for the rate constant for rISC (k_{rISC}) as modified by Parker *et al.*[27] in terms of a thermal equilibrium between the S_1 and T_1 states is given as[28]

$$k_{rISC} = \frac{1}{3} k_{ISC} \exp(-\Delta E_{S_1-T_1} / k_B T) \qquad (2)$$

The factor 1/3 is due to the thermal averaging of the contribution of all the three spin sublevels of the T_1 state. $\Delta E_{S_1\text{-}T_1}$ is the energy gap between the S_1 and T_1 states, $k_B$isthe Boltzmann constant, and T denotes temperature, which in our case is 300K. The k_{rISC} obtained from equation 2 is 7.02 $\times 10^4\ s^{-1}$(Table 1), more than 3×10^4 times slower than k_{ISC}. This suggests efficient population gain of the T_1 state, satisfying the fundamental condition for triplet lasing, and simultaneously avoiding any possibility of TADF.[26] To drive population transfer from the T_1 state, there still exist two more challenges: a long lifetime of the triplet states and a strong $T_1 \rightarrow T_n$ absorption.

Table 1. Rate constant for S_1-T_1 ISC [$k_{ISC}(s^{-1})$], rate constant for S_1-T_1 rISC [$k_{rISC}(s^{-1})$], radiative rate constant for the $T_1 \rightarrow S_0$ transition [$k_r(s^{-1})$], nonradiative rate constant for the $T_1 \rightarrow S_0$ transition [$k_{nr}(s^{-1})$]and the computed lifetime [τ_r (μs)] of S-BF_2.

System	k_{ISC}	k_{rISC}	k_r	k_{nr}	τ
S-BF_2	2.26×10^9	7.02×10^4	0.24	9.6×10^5	1.03

To estimate the lifetime (τ) of the T_1 state of S-BF_2, we have evaluated the radiative (k_r) and nonradiative (k_{nr}) rate constants, as τ is given by the expression $1/(k_r+k_{nr})$. k_r is calculated assuming the high-temperature limit approximation[29] where all three sub-levels of the triplet manifold contribute equally in the phosphorescence process. Also, the 0−0 FC overlap factor (4.3×10^{-6}) considering vibronic influence, and the Strickler−Berg correction[30] because of CH_2Cl_2 solvent (refractive index of $CH_2Cl_2$is 1.424), has been applied in the computation of k_r and the detailed expression is provided in the Supporting Information. k_{nr} is evaluated utilizing equation 1. The SOC matrix elements $\langle T_1|H_{SO}|S_0\rangle = 5.6\ cm^{-1}$, $\Delta E_{T_1\text{-}S_0} = 2.19$ eV and FCWD is estimated following the same method as used for k_{ISC}. The calculated k_r and k_{nr} and the net lifetime are reported in Table 1. The small k_r value at the single molecule level indicates that aggregation-induced enhancement of photoluminescence might play an important role to determine the net photoluminescence quantum yield.[31] Nevertheless,Table 1 reveals that the lifetime of S-BF_2 is 1.03 μs, consistent with the experimental data (8.3 ± 0.1 μs in 1×10^{-5} M CH_2Cl_2 and 9.3 ± 0.4 μs in the solid state). It was earlier reported that metal-free organic compounds such as simple arylboronic esters[32] and triazine derivatives[20] are likely to exhibit ultralong lifetimes (>1 s). The lifetime observed for S-BF_2 is instead a boon in the context of lasing because it removes the likelihood of TTA since TTA usually occurs if the triplet state lifetime is in the range of 30 μs.[33] We recall that in addition to TTA, triplet exciton-polaron annihilation (TPA) often becomes very important and acts as a major quenching mechanism in OLED. However, the rate of TTA may, depending on the nature of the materials, exceed the rate of TPA both in OSSL and OLED.[34-36] Due to the lack of experimental data on the TPA of this material and the dominant

role of TTA in OSSL as evidenced from the existing literature,[35,36] we did not conduct any additional ab initio investigations of TPA.

Finally, we consider the key issue of the spin-allowed $T_1 \rightarrow T_n$ absorption process which often overlaps with the $T_1 \rightarrow S_0$ emission. Triplet lasing is possible under the simple condition that the stimulated emission cross section ($\sigma_{em(T_1 \rightarrow S_0)}$) exceeds the triplet-triplet absorption cross section ($\sigma_{TT(T_1 \rightarrow T_n)}$) at a particular wavelength.[37] To verify that this applies to S-BF_2, we have computed S_0-S_n absorption, $T_1 \rightarrow S_0$ emission and $T_1 \rightarrow T_n$ absorption for the tetramer of S-BF_2 in an arrangement that resembles the unit cell of this crystalline material. Since the calculations at the CASSCF/NEVPT2[14]level are hardly feasible for a tetramer, we have performed all these calculations on the optimized geometries of S_0 and T_1 at the TDDFT level of theory using Dunning's cc-pVDZ basis[15] in combination with the range-separated ω-B97XD functional.[38] The computed phosphorescence wavelength is found to be 675 nm, which is quite close to the experimental triplet lasing wavelength (650 nm). The CASSCF/NEVPT2[14]+ RIJCOSX[39] computation on a dimer also yields a reasonably satisfactory phosphorescence wavelength(626 nm). Interestingly, we have found that the phosphorescence from the tetramer exhibits significant charge-transfer character, which is responsible for the large red shift in the phosphorescence wavelength compared to the monomer. Besides, the calculated T_1-T_n gap for the 50 triplet states of the tetramer suggests that there would be no triplet-triplet absorption for wavelengths of 635-710 nm, whereas CASSCF/NEVPT2[14]+ RIJCOSX[39] calculations on the optimized dimer reveal that the intense triplet-triplet absorption will occur at 470 nm. This fundamental finding indicates that the triplet-triplet absorption cross section at the triplet lasing

wavelength will be practically zero, providing decisive evidence that large T_1-S_0 emission cross section from S-BF_2can be achieved.

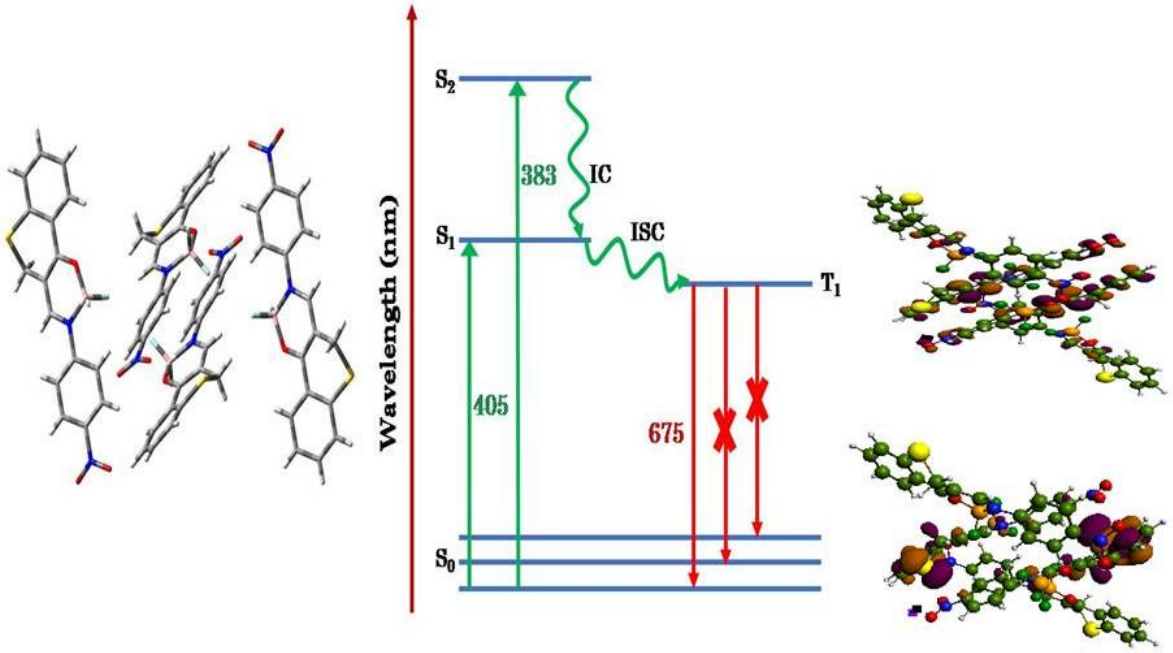

Figure4. Optimized geometry of the tetramer of S-BF_2 and the computed wavelength of different absorption and emission processes. The four levels involved in the lasing mechanism are S_0-S_2-S_1-T_1. The vertical lines with a cross(red) indicated the non-existence of 0-1 or other vibronic components of the emission.

In summary, we have presented a molecular mechanism for the origin of triplet lasing from S-BF_2, effectively delivering the first design principles for the development of new organic solid-state triplet lasing materials. S-BF_2achieves population inversion between the T_1 and S_0 states, aided by several photo-physical processes. The faster k_{ISC} compared to k_{rISC} for the $S_1 \rightarrow T_1$ transition prevents TADF. Moreover, k_{ISC} for $S_1 \rightarrow T_1$ is much larger than the non-radiative

decay rate of T_1-S_0. Furthermore, whereas the moderate lifetime restricts TTA of the triplet excitons, poor vibronic coupling ensures coherent emission from the T_1 state. The large separation of the$T_1 \rightarrow T_n$ absorption and T_1-S_0 emission spectra indicates that intense stimulated emission is very likely from S-BF_2. Finally, the fine tuning of the above factors garnered together can be used to probe the possible triplet lasing property of a molecule.

ASSOCIATED CONTENT

Supporting Information.

The Supporting information is available free of charge.

(1) Computational details. (2) Co-ordinates of the optimized geometries of S-BF_2. (3) Structural parameters. (4) Estimation of Franck-Condon (FC) integrals. (5) Calculation of the rate constant for$S_1 \rightarrow T_1$ and $S_1 \rightarrow T_2$ intersystem crossing (ISC) [k_{ISC}]. (6) Expression for the radiative rate constant (k_r) for the $T_1 \rightarrow S_0$ electronic transitions.7) Optimized coordinates of the ground state singlet and triplet of the tetramer of S-BF_2.(PDF)

AUTHOR INFORMATION

Notes

The authors declare no competing financial interests.

ACKNOWLEDGMENT

L.P. thanks the Council of Scientific and Industrial Research (CSIR) for granting her the Senior Research Fellowship.

REFERENCES

(1) Wohlgenannt, M.; Tandon, K.; Mazumdar, S.; Ramasesha, S; Vardeny, Z. V. Formation Cross-Sections of Singlet and Triplet Excitons in π-Conjugated Ploymers. *Nature***2001**, *409*, 494-497.

(2) Bakulin, A. A.; Rao, A.; Pavelyev, V. G.; van Loosdrecht, P. H.; Pshenichnikov, M. S.; Niedzialek, D.; Cornil, J.; Beljonne, D.; Friend, R. H. The Role of Driving Energy and Delocalized States for Charge Separation in Organic Semiconductors. *Science***2012**, *335*, 1340-1344.

(3) Xing, G.; Mathews, N.; Sun, S.; Lim, S. S.; Lam, Y. M.; Grätzel, M.; Mhaisalkar, S.; Sum, T. C. Long-Range Balanced Electron and Hole-Transport Lengths in Organic-Inorganic $CH_3NH_3PbI_3$. *Science***2013**, *342*, 344-347.

(4) Hill, M. T.; Gather, M. C. Advances in Small Lasers. *Nat. Photonics***2014**, *8*, 908-918.

(5) Yu, Z.; Wu, Y.; Liao, Q.; Zhang, H.; Bai, S.; Li, H.; Xu, Z.; Sun, C.; Wang, X.; Yao, J.; Fu, H. Self-Assembled Microdisk Lasers of Perylenediimides. *J. Am. Chem. Soc.* **2015**, *137*, 15105-15111.

(6) Yu, Z.; Wu, Y.; Xiao, L.; Chen, J.; Liao, Q.; Yao, J.; Fu, H. Organic Phosphorescence Nanowire Lasers. *J. Am. Chem. Soc.* **2017**, *139*, 6376-6381.

(7) Grivas, C.; Pollnau, M. Organic Solid-State Integrated Amplifiers and Lasers.*Laser Photoincs Rev.***2012**, *6*, 419-462.

(8) Vahtras, O.; Ågren, H.; Jørgensen, P.; Jensen, H. J. A.; Helgaker, T.; Olsen, J. Spin-Orbit Coupling Constants in a Multiconfiguration Linear Response Approach. *J. Chem. Phys.***1992**, *96*, 2118-2126.

(9) Manchon, A.; Koo, H. C.; Nitta, J.; Frolov, S. M.; Duine, R. A. New Perspectives for Rashba Spin-Orbit Coupling. *Nat. Mater.* **2015**, *14*, 871-882.

(10) Birks, J. B. *Photophysics of Aromatic Molecules*; Wiley-Interscience: New York, 1970.

(11) Smith, M. B.; Michl, J. Singlet Fission. *Chem. Rev.* **2010**, *110*, 6891-6936.

(12) Zhao, Y. S.; Fu, H.; Peng, A.; Ma, Y.; Liao, Q.; Yao, J. Construction and Optoelectronic Properties of Organic One-Dimensional Nanostructures. *Acc. Chem. Res.* **2010**, *43*, 409-418.

(13) Furche, F.; Ahlrichs, R. Adiabatic Time-Dependent Density Functional Methods for Excited State Properties. *J. Chem. Phys.* **2002**, *117*, 7433-7447.

(14) Angeli, C.; Cimiraglia, R.; Evangelisti, S.; Leininger, T.; Malrieu, J. P. Introduction of N-Electron Valence States for Multireference Perturbation Theory. *J. Chem. Phys.* **2001**, *114(23)*, 10252-10264.

(15) Dunning, T. H. J. Gaussian Basis Sets for Use in Correlated Molecular Calculations. I. The Atoms Boron Through Neon and Hydrogen. *Chem. Phys.* **1989**, *90*, 1007-1023.

(16) Berning, A.; Schweizer, M.; Werner, H. J.; Knowles, P. J.; Palmieri, P. Spin-Orbit Matrix Elements for Internally Contracted Multireference Configuration Interaction Wavefunctions. *Mol. Phys.* **2000**, *98(21)*, 1823-1833.

(17) Tomasi, J.; Mennucci, B.; Cammi, R. Quantum Mechanical Continuum Solvation Models. *Chem. Rev.* **2005**, *105*, 2999-3094.

(18) Kleinschmidt, M.; Wüllen, C. V.; Marian, C. M. Intersystem-Crossing and Phosphorescence Rates in fac-$Ir^{III}(ppy)_3$: A Theoretical Study Involving Multi-Reference Configuration Interaction Wavefunctions. *J. Chem. Phys.* **2015**, *142*, 94301-94316.

(19) Marian, C. M. Spin-Orbit Coupling and Intersystem Crossing in Molecules. *WIREsComput. Mol. Sci.***2012**, *2*, 187-203.

(20) Paul, L.; Chakrabarti, S.; Ruud, K.; Origin of Dual-Peak Phosphorescence and Ultralong Lifetime of 4,6-Diethoxy-2-carbazolyl-1,3,5-triazine. *J. Phys. Chem. Lett.***2017**, *8*, 1253-1258.

(21) Baryshnikov, G.; Minaev, B.; Ågren, H. Theory and Calculation of the Phosphorescence Phenomenon. *Chem. Rev.* **2017**, *117*, 6500-6537.

(22) Minaev, B.; Baryshnikov, G.; Ågren, H. Principles of Phosphorescent Organic Light Emitting Devices. *Phys. Chem. Chem. Phys.* **2014**, *16*, 1719-1758.

(23) Brédas, J. L.; Beljonne, D.; Coropceanu, V.; Cornil, J. Charge-Transfer and Energy-Transfer Processes in Pi-Conjugated Oligomers and Polymers: A Molecular Picture. *Chem. Rev.* **2004**, *104*, 4971-5003.

(24) Tong, G. S. M.; Chan, K. T.; Chang, X.; Che, C. Theoretical Studies on the Photophysical Properties of Luminescent PinserGold(III) Arylacetylide Complexes: The Role of π-Conjugation at the C-Deprotonated [C^N^C] Ligand. *Chem. Sci.* **2015**, *6*, 3026-3037.

(25) Jong, M. D.; Seijo, L.; Meijerink, A.; Rabouw, F. T. Resolving the Ambiguity in the Relation between Stokes Shift and Huang-Rhys Parameter. *Phys. Chem. Chem. Phys.* **2015**, *17*, 16959-16969.

(26) Chen, T.; Zheng, L.; Yuan, J.; An, Z.; Chen, R.; Tao, Y.; Li, H.; Xie, X.; Huang, W. Understanding the Control of Singlet-Triplet Splitting for Organic Exciton Manipulating: A Combined Theoretical and Experimental Approach. *Sci. Rep.* **2015**, *5*, 10923-10934.

(27) Parker, C. A.; Hatchard, C. G. Triplet-Singlet Emission in Fluid Solutions. Phosphorescence of Eosin. *Trans.Faraday Soc.* **1961**, *57*, 1894-1904.

(28) Gibson, J.; Monkman, A. P.; Penfold, T. J. The Importance of Vibronic Coupling for Efficient Reverse Intersystem Crossing in Thermally Activated Delayed Fluorescence Molecules. *ChemPhysChem***2016**, *17*, 2956-2961.

(29) Younker, J. M.; Dobbs, K. D. Correlating Experimental Photophysical Properties of Iridium(III) Complexes to Spin-Orbit Coupled TDDFT Predictions. *J. Phys. Chem. C***2013**, *117*, 25714-25723.

(30) Mori, K.; Goumans, T. P. M.; Lenthe, E. V.; Wang, F. Predicting Phosphorescent Lifetimes and Zero-Field Splitting of Organometallic Complexes with Time-Dependent Density Functional Theory Including Spin-Orbit Coupling. *Phys. Chem. Chem. Phys.***2014**, *16*, 14523-14530.

(31) Mei, J.; Leung N.L.C.; Kwok, R.T.K.; Lam, J.W.Y.; Tang, B.Z. Aggregation-Induced Emission: Together We Shine, United We Soar! *Chem. Rev.***2015**, *115*, 11718-11940.

(32) Shoji, Y.; Ikabata, Y.; Wang, Q.; Nemoto, D.; Sakamoto, A.; Tanaka, N.; Seino, J.; Nakai, H.; Fukushima, T. Unveiling a New Aspect of Simple Arylboronic Esters: Long-Lived Room-Temperature Phosphorescence from Heavy-Atom-Free Molecules. *J. Am. Chem. Soc.* **2017**, *139*, 2728-2733.

(33) Yu, J.; Lammi, R.; Gesquiere, A. J.; Barbara, P. F. Singlet-Triplet and Triplet-Triplet Interactions in Conjugated Polymer Single Molecules. *J. Phys. Chem. B***2005**, *109*, 10025-10034.

(34) Lee, J.; Chen, H.F.; Batagoda, T.; Coburn, C.; Djurovich, P.I.; Thompson, M.E.; Forrest, S.R. Deep Blue Phosphorescent Organic Light-Emitting Diodes with Very High Brightness and Efficiency. *Nat. Mater.*, **2016**, *15*, 92-98.

(35) Lehnhardt, M.; Riedl, T.; Weimann, T.; Kowalsky, W. Impact of Triplet Absorption and Triplet-Singlet Annihilation on the Dynamics of Optically Pumped Organic Solid-State Lasers. *Phys. Rev. B*, **2010**, *81*, 165206.

(36) Hale, G.D.; Oldenburg, S.J.; Halas, N.J. Observation of Triplet Exciton Dynamics in Conjugated Polymer Films Using Two-Photon Photoelectron Spectroscopy. *Phys. Rev. B*, **1997**, *55*, R16069.

(37) Forget, S.; Chénais, S. *Organic Solid-State Lasers*; Springer-Verlag: Berlin Heidelberg 2013.

(38) Chai, J.D.; Head-Gordon, M. Long-Range Corrected Hybrid Density Functionals with Damped Atom-Atom Dispersion Corrections. *Phys. Chem. Chem. Phys.***2008**, *10*, 6615-6620.

(39) Izsák, R.; Neese, F. An Overlap Fitted Chain of Spheres Exchange Method. *J. Chem. Phys.* **2011**, *135*, 144105.